Letter

Circuit realization of a tilted Dirac cone: Platform for fabrication of curved spacetime geometry on a chip

Ahmad Motavassal[*] and S. A. Jafari ®[†]

Department of Physics, Sharif University of Technology, Tehran 11155-9161, Iran

We present an *LC* circuit model that supports a tilted "Dirac cone" in its spectrum. The tilt of the Dirac cone is specified by the parameters of the model consisting of mutual inductance between the neighboring sites and a capacitance C_0 at every lattice site. These parameters can be completely measured by impedance spectroscopy. Given that a tilted Dirac cone can be described by a background spacetime metric, the impedance spectroscopy can perfectly provide (local) information about the metric of the spacetime. Nonuniform spatial dependence of the mutual inductance or capacitance induces a nontrivial geometrical structure on the emergent spacetime. Our work extends the range of usefulness of circuit models to emulate nontrivial spacetime structures.

DOI: 10.1103/PhysRevB.104.L241108

Introduction. The dynamics of electrons in solids is shaped by the lattice structure on which they are mounted [1]. The constituent electron/ion system cannot be separated from the underlying lattice. Circuit electrodynamics offers an alternative to place circuit elements on complicated lattices. For example, the topology of electron bands of solids can be emulated by circuits [2,3]. But lattices can offer more than band topology: A lattice first breaks the Poincaré group [4] into one of 230 possible space groups (SGs) [5]. Hence the elementary excitations in the solids can be drastically distinct from those in elementary particle physics [6]. The irreducible representations of the SG do not allow the band structures to arbitrarily disperse and restricts them by the compatibility relations of little groups of various high-symmetry points/lines/surfaces [7]. Breaking the Poincaré group [4] also invalidates the spin-statistics theorem [4,6] and hence on some lattices fermions may belong to nonspinor representations [8], such as a spin-1 representation known as triple fermions [9]. As we will see shortly, the reverse is also possible and a bosonic theory can acquire a spinor representation.

Lattices offer yet another fascinating perspective: It appears that the continuum limit of certain SGs corresponds to a spacetime geometry (metric) as detailed below. A simple nearest-neighbor model of fermions hopping on the honeycomb lattice describes the Dirac fermions of graphene [10] that can be interpreted as an emergent Minkowski spacetime. It turns out that in certain materials—notably the 8*Pmmn* borophene that belongs to SG number 59—the Dirac cone gets tilted [11–14]. The tilting can be embedded into an emergent metric [15–20] $ds^2 = -v_F^2 dt^2 + (dr - \zeta v_F dt)^2$, where v_F replaces the speed of light c and is the velocity scale for this emergent spacetime. In two space dimensions with

$\boldsymbol{\zeta} = (\zeta_x, \zeta_y)$, one has

$$g_{\mu\nu} = \begin{bmatrix} -1 + \zeta^2 & \zeta_x & \zeta_y \\ \zeta_x & 1 & 0 \\ \zeta_y & 0 & 1 \end{bmatrix},$$

$$g^{\mu\nu} = \begin{bmatrix} -1 & -\zeta_x & -\zeta_y \\ -\zeta_x & 1 - \zeta_x^2 & -\zeta_x\zeta_y \\ -\zeta_y & -\zeta_x\zeta_y & 1 - \zeta_y^2 \end{bmatrix},$$

where $\zeta^2 = \zeta_x^2 + \zeta_y^2$ and the above two matrices are the inverse of each other [21,22]. ζ appears as a redshift factor in many quantities, including the density of states [23]. At $\boldsymbol{\zeta} = 0$, the above metric reduces to $\eta_{\mu\nu} = \text{diag}(-1, 1, 1)$.

The relation between the *space* geometry and certain graphs is well known [24–26]. Hence it is feasible that the dynamics on certain SGs mimics an emergent spacetime. The purpose of this Letter is to present an *LC* circuit model on which the dynamics of the voltage and current at long time/distances is governed by the above metric. We will show how the "square root" of the resulting Klein-Gordon equation is equivalent to a theory of tilted Dirac fermions. The same tilted Dirac theory emerges in electron theories of 8*Pmmn* borophene [27]. This suggests that the resulting Dirac theory is a property of the underlying lattice.

Honeycomb lattice circuit model. Inspired by our coarse grained [28,29] fermionic model introduced in Ref. [27], in Fig. 1 we consider an *LC* circuit based on the periodic honeycomb lattice. Here, L_0 (black) denotes inductance between the nearest neighbors. The second neighbor inductances are of two types, L_1 (blue) and L_2 (red). The third neighbors along the horizontal direction are connected with L_3 (green). Every site is grounded by a capacitance C_0. The inductance connection enriches the graph structure of a simple honeycomb lattice similar to an effective fermionic hopping model [2], where the further neighbor connections set the location [30] and tilt [27] of the Dirac cone. The honeycomb lattice is composed of two Bravais sublattices A and B [10]. Setting the length of a bond by $a_0 = 1/\sqrt{3}$, the primitive lattice
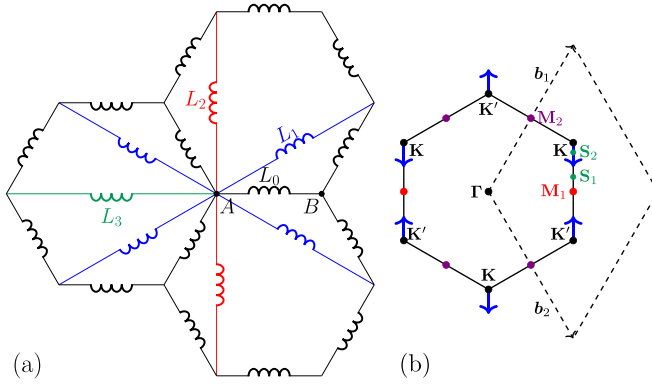
*ahmad.motavassal@gmail.com
†jafari@sharif.edu

FIG. 1. (a) The structure of a honeycomb circuit. Curly lines of various colors indicate the inductance between various neighbors. For clarity only the neighbors of a single site are drawn. Every node of the lattice is grounded by a capacitance C_0. (b) Brillouin zone in both Wigner-Seitz (solid honeycomb) and primitive cell (dashed rhombus) constructions. The reciprocal vectors b_1 and b_2 are shown. The blue arrows show the direction of movement of the Dirac nodes when we vary L_3. The red and purple points label the saddle points M_1 and M_2 (see the text). Two other possible extrema denoted by green S_1 and S_2 are vertically displaced from a Dirac point on both sides.

vectors are $a_{1|2} = (\sqrt{3}, \pm 1)/2$. Corresponding reciprocal lattice vectors depicted in Fig. 1(b) are $b_{1|2} = 2\pi(1, \pm\sqrt{3})/\sqrt{3}$. Suppose that the voltage at site r at time t in sublattice A(B) is $V_{1(2)}(r, t)$. The Kirchhoff current law for site A reads

$$\sum_{\delta} \frac{V_1(r) - V_2(r+\delta)}{L_0} + \sum_{i,\lambda} \frac{V_1(r) - V_1(r+\lambda a_i)}{L_1}$$
$$+ \sum_{\lambda} \frac{V_1(r) - V_1(r + \lambda(a_1 - a_2))}{L_2}$$
$$+ \frac{V_1(r) - V_2(r - a_1 - a_2)}{L_3} + C_0 \frac{d^2 V_1(r)}{dt^2} = 0,$$

where δ runs over the three first neighbors, and $i = 1, 2$ labels the basis vectors a_1 and a_2, $\lambda = \pm$. A similar equation for sublattice B can be written by $\delta \to -\delta$ and $a_i \to -a_i$. Harmonic solutions of the type $V_i(r, t) = V_i(r)e^{-i\omega t}$ subject to translational invariance $V_i(r) = V_i(k)e^{ik\cdot r}$ give

$$V_1(k)[\nu_0 - 2a(\cos k \cdot a_1 + \cos k \cdot a_2) - 2b\cos k \cdot (a_1 - a_2)]$$
$$- V_2(k)[(1 + e^{-ik\cdot a_1} + e^{-ik\cdot a_2}) - ce^{-ik\cdot(a_1+a_2)}]$$
$$= \bar\omega^2 V_1(k),$$

where we have defined dimensionless (and positive) parameters $a = \frac{L_0}{L_1}$, $b = \frac{L_0}{L_2}$, $c = \frac{L_0}{L_3}$, and $\nu_0 = 3 + 4a + 2b + c$. The frequency $\omega_*^2 = (L_0 C_0)^{-1}$ is the natural frequency of the system that allows us to define the dimensionless frequency $\bar\omega$ by $\omega = \omega_* \bar\omega$. Putting together the equations for A and B results in the eigenvalue problem for the *dynamical matrix* $D(k)$,

$$\begin{pmatrix} \varepsilon(k) & \Delta(k) \\ \Delta^*(k) & \varepsilon(k) \end{pmatrix} \begin{pmatrix} V_1(k) \\ V_2(k) \end{pmatrix} = \bar\omega^2(k) \begin{pmatrix} V_1(k) \\ V_2(k) \end{pmatrix}, \quad (1)$$

where $\varepsilon(k) = \nu_0 - 4a \cos k_x \frac{\sqrt{3}}{2} \cos \frac{k_y}{2} - 2b \cos k_y$ and $\Delta(k) = |\Delta|e^{i\phi} = -1 - 2e^{-ik_x \frac{\sqrt{3}}{2}} \cos \frac{k_y}{2} - ce^{-ik_x\sqrt{3}}$. Despite that quantization of the current-voltage oscillator gives a bosonic theory, a spinor structure naturally emerges from the two-sublattice nature of the honeycomb lattice $\langle V_k| = (V_1(k) \; V_2(k))$. Equation (3) gives $\bar\omega_\pm^2(k) = \varepsilon(k) \pm |\Delta(k)|$ and $|V_{\pm,k}\rangle = \frac{1}{\sqrt{2}}\binom{\pm e^{i\phi}}{1}$, where ϕ is the phase of the complex number Δ. The splitting between the upper (+) and lower (−) frequency bands is controlled by $\Delta(k)$ where

$$|\Delta(k)|^2 = 4\left[\cos^2 \frac{k_y}{2} + (1+c)\cos \frac{k_y}{2} \cos \frac{k_x\sqrt{3}}{2}\right.$$
$$\left. + c\cos^2 \frac{k_x\sqrt{3}}{2} + \left(\frac{1-c}{2}\right)^2\right]. \quad (2)$$

The upper and lower bands meet when $0 \leqslant c \leqslant 1$ (see Supplemental Material [31] for details). When $c = 0$, the gap closing points (nodes) are located on the corners of the Brillouin zone (BZ) as shown in Fig. 1(b) in the Wigner-Seitz and primitive cell representations. The coordinates of $\mathbf{K}/\mathbf{K}'$ are $(0, \mp 4\pi/3)$. Upon increasing c, the horizontal coordinates of these points do not change, but because of the increase in $\cos \frac{k_y}{2}$, $\mathbf{K}$ and $\mathbf{K}'$ move vertically towards each other. Hence the role of parameter c is to control the location of the two independent (see the rhombus primitive cell BZ) nodes. Increasing c from 0 to 1 *shifts* the two nodes toward each other. At $c = 1$ these two points collide and annihilate at the M_1 point—due to their opposite topological charge—giving a fully gapped spectrum for $c > 1$.

Dirac theory. $\varepsilon(k)$ and $\Delta(k)$ near the gap closing point become

$$\varepsilon(k) \approx \bar\omega_0^2 + \tau\alpha_y\delta k_y, \quad \Delta \approx -iw_x\delta k_x + \tau w_y\delta k_y,$$
$$\bar\omega_0^2 = (3+c)[1 + 2a + b(1-c)], \quad (3)$$

where $\tau = \pm$ marks the node (valley) around which the linearization has been made, $(\delta k_x, \delta k_y)$ are the deviations from the gap closing point, and $\alpha_y = \sqrt{(1-c)(3+c)}[a - b(1 + c)]$ while $w_x = \sqrt{3}(1-c)/2$ and $w_y = \sqrt{(1-c)(3+c)}/2$ that determine the dynamical matrix (1). By a Taylor expansion of the square root of the matrix $D(k)$ around $\bar\omega_0^2$, one obtains a new matrix $h(k)$ whose eigenvalues are $\bar\omega(k)$:

$$h(k) = (\bar\omega_0 + v_t \cdot \delta k)\sigma_0 + (-iv_x\delta k_x\sigma_x + \tau v_y\delta k_y\sigma_y),$$
$$v_x = \frac{w_x}{2\bar\omega_0}, \quad v_y = \frac{w_y}{2\bar\omega_0}, \quad v_{ty} = \frac{\alpha_y}{2\bar\omega_0}, \quad v_{tx} = 0, \quad (4)$$

where v_t is the "tilt" velocity scale that defines the tilt parameter by $\zeta_a = v_{ta}/v_a$, $a = x, y$. Therefore, close to the operation frequency $\bar\omega_0$ given by Eq. (3), the matrix, whose eigenvalues give the eigenfrequencies of our circuit system are given in Eq. (4), describes tilted Dirac fermions. The above tilted Dirac theory can be regarded as the "square root" of theory described by $D(k)$, the same way that the Dirac equation is regarded as the square root of the Klein-Gordon equation [4]. The square root operation connecting mechanical/bosonic systems with corresponding fermionic systems can be properly defined on the lattice as well [32,33].

TABLE I. Extrema and their corresponding values of Ω.

	$\boldsymbol{k}$	$\Omega_\pm$	Type
$\boldsymbol{\Gamma}$	$(0,0)$	$0, 6+2c$	Max/Min
$\mathbf{M}_1$	$(\pm\frac{2\pi}{\sqrt{3}}, 0)$	$2+8a+2c, 4+8a$	Saddle
$\mathbf{M}_2$	$(\pm\frac{\pi}{\sqrt{3}}, \pm\pi)$	$2+4a+4b+2c, 4+4a+4b$	Saddle
$\mathbf{S}_1$	$[\pm\frac{2\pi}{\sqrt{3}}, 2\cos^{-1}(\mp\frac{1+2a}{4b})]$	$\frac{1}{4b}(1+2a+4b)^2$	Max/Min
$\mathbf{S}_2$	$[\pm\frac{2\pi}{\sqrt{3}}, 2\cos^{-1}(\mp\frac{1-2a}{4b})]$	$2c+6+\frac{1}{4b}(-1+2a+4b)^2$	Max/Min

Spectral density. For the rest of this Letter we do not need $h(\boldsymbol{k})$ and continue to work with $D(\boldsymbol{k})$. So we define a new symbol $\Omega(\boldsymbol{k}) = \bar{\omega}^2(\boldsymbol{k})$ to label its eigenvalues. This is because the impedance spectroscopy will directly measure the spectrum of the $D(\boldsymbol{k})$, not the Dirac Hamiltonian (4). The resolvent [34] of the $D(\boldsymbol{k})$ that describes the dynamics of the voltage/current on the graph is

$$G(\boldsymbol{k}, z) = \frac{1}{2} \frac{1}{[z-\varepsilon(\boldsymbol{k})]^2 - |\Delta(\boldsymbol{k})|^2} \begin{pmatrix} z-\varepsilon(\boldsymbol{k}) & \Delta(\boldsymbol{k}) \\ \Delta^*(\boldsymbol{k}) & z-\varepsilon(\boldsymbol{k}) \end{pmatrix},$$

the imaginary part of which is defined by $\rho = -\frac{1}{\pi}\mathrm{Im}\{\mathrm{tr}[G^+]\}$, where $G^+(\boldsymbol{k}, \lambda) = G(\boldsymbol{k}, \lambda + i0^+)$ gives the density of states (DOS). The trace includes a summation over the diagonal elements of G and integration over the whole BZ.

When the spectral density is plotted as a function of Ω, it contains a great deal of information. The first important feature of the density of Ω values is the location of the Dirac node [Eq. (3)] $\bar{\omega}_0^2 = \Omega_0$ that corresponds to $\Omega_+(\boldsymbol{k}) = \Omega_-(\boldsymbol{k})$. This gives the first relation among the model parameters a, b, c that can be directly read off from the DOS. The extrema of DOS are determined from $\nabla_{\boldsymbol{k}}\Omega(\boldsymbol{k}) = 0$ (see Supplemental Material [31] for details). In Table I we list the positions and values of Ω at two van Hove singularities $\mathbf{M}_1$ and $\mathbf{M}_2$ shown in Fig. 1(b). Because $\mathbf{M}_1$ and $\mathbf{M}_2$ are saddle points, they give logarithmic van Hove singularities whose locations directly relate to the model parameters as

$$(\Omega_+ - \Omega_-)|_{\mathbf{M}_1} = (\Omega_+ - \Omega_-)|_{\mathbf{M}_2} = 2(1-c), \quad (5)$$

$$\Omega_+|_{\mathbf{M}_2} - \Omega_+|_{\mathbf{M}_1} = \Omega_-|_{\mathbf{M}_2} - \Omega_-|_{\mathbf{M}_1} = 4(b-a). \quad (6)$$

The first equation tells us that the van Hove singularities arising from a given point in the upper and lower branches are separated by deviations of c from 1. This helps to immediately read off the parameter c. The second equation above implies that the separation of van Hove singularities in the upper branch is controlled by $b - a$, and when $a = b$ the van Hove singularities for $\mathbf{M}_1$ and $\mathbf{M}_2$ points coincide and hence the number of van Hove singularities is reduced by two. Now let us see how one can measure the location of the above singularities.

Impedance spectroscopy. This measurement consists in sending a current through one node into our *LC* lattice and extracting the current through another (arbitrary) node, which corresponds to adding a nonzero current to the right-hand side of Eq. (1) [35]. The operation frequency can be adjusted at will to probe the Dirac physics near the crossing point Ω_0. If the current is sent in to site $\boldsymbol{r}_a$ on sublattice ν_1 and is extracted from site $\boldsymbol{r}_b$ on sublattice ν_2, then one has to add $I_\nu(\boldsymbol{r}) = I_0[\delta_{\nu\nu_1}\delta(\boldsymbol{r} - \boldsymbol{r}_a) - \delta_{\nu\nu_2}\delta(\boldsymbol{r} - \boldsymbol{r}_b)]$ or in Fourier representation $I_\nu(\boldsymbol{k}) = I_0(\delta_{\nu\nu_1}e^{-i\boldsymbol{k}\cdot\boldsymbol{r}_a} - \delta_{\nu\nu_2}e^{-i\boldsymbol{k}\cdot\boldsymbol{r}_b})$ to the right-hand

side of Eq. (1) that gives $[D(\boldsymbol{k}) - \Omega\sigma_0]|V\rangle = -i\omega L_0|I(\boldsymbol{k})\rangle$. By $D(\boldsymbol{k}) - \Omega\sigma_0 = -G^{-1}(\boldsymbol{k}, \Omega)$, we obtain the matrix equation $V_\mu = i\omega L_0 G_{\mu\nu}I_\nu$ where $\mu, \nu = 1, 2$ label the sublattices. By the definition of impedance (the difference between the voltages of the nodes divided by the current) we get

$$Z_{\nu_1\nu_2}(\boldsymbol{r}_a - \boldsymbol{r}_b) = i\omega_* L_0 \sqrt{\Omega} \frac{1}{N} \sum_{\boldsymbol{k}} \big[G_{\nu_1\nu_1} + G_{\nu_2\nu_2}$$
$$- G_{\nu_1\nu_2}e^{i\boldsymbol{k}\cdot(\boldsymbol{r}_a - \boldsymbol{r}_b)} - G_{\nu_2\nu_1}e^{-i\boldsymbol{k}\cdot(\boldsymbol{r}_a - \boldsymbol{r}_b)}\big], \quad (7)$$

where N is the number of unit cells. The frequency dependence is implied for the Green's function matrix elements $G_{\nu_i\nu_j}$. For large enough lattices with many degrees of freedom, the sum over $\boldsymbol{k}$ can be replaced by an integral over BZ. This completes the expression of the impedance in terms of the Green's function. It further suggests to work with the "normalized impedance" $Z_{\nu\nu}/(\omega_* L_0)$. As can be seen in Fig. 2, the (local) impedance measured between typical in-out points separated by $\boldsymbol{a}_1$ clearly contains information about the essential features of the DOS and hence serves as a spectroscopic determination tool to measure the a, b, c parameters. If one probes the *nonlocal* impedance between arbitrary unit cells separated by $\boldsymbol{r}_a - \boldsymbol{r}_b = m\boldsymbol{a}_1 + n\boldsymbol{a}_2 = [(m+n)\sqrt{3}/2, (m-n)/2]$, the diagonal component of Eq. (7) gives

$$\sum_{\boldsymbol{k}} 2G_{\nu_1\nu_1}(1 - \cos[\boldsymbol{k}\cdot(\boldsymbol{r}_a - \boldsymbol{r}_b)]) = \sum_{\boldsymbol{k}} 2G_{\nu_1\nu_1}\Delta\phi. \quad (8)$$
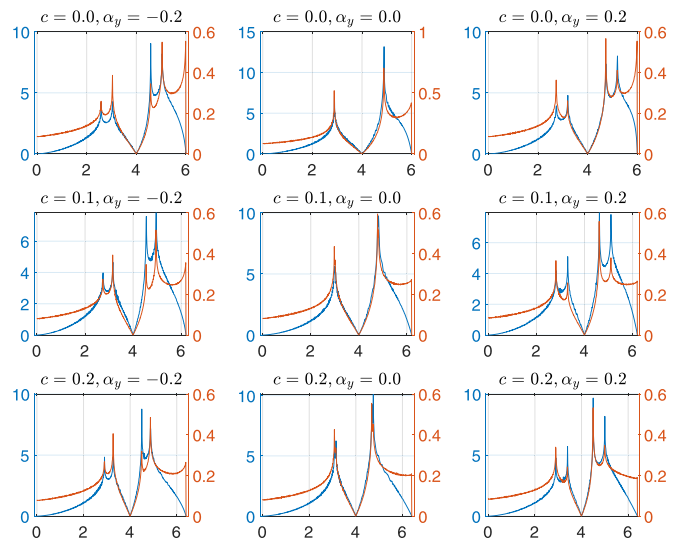

FIG. 2. The impedance and DOS curves vs Ω for different values of c and α_y. The Dirac level Ω_0 is held fixed at 4. The blue (orange) curve with the axis range on the left (right) is $\mathrm{Re}\{Z_{AA}(\boldsymbol{a}_1)\}$ (DOS).

TABLE II. *Selection rules* for the DOS singularities in impedance spectroscopy. $\checkmark$/$\times$ indicate the presence/absence of the DOS singularity.

Parity of (m, n)	$\mathbf{M}_1$	$\mathbf{M}_2$
(even, even)	$\times$	$\times$
(odd, odd)	$\times$	$\checkmark$
(even, odd) or (odd, even)	$\checkmark$	$\checkmark$

The term in the parentheses denoted by $\Delta\phi$ resembles the atomic interference term that arises in the scattering determination of crystal structure [36]. For $k_{\mathbf{M}_1} = (\pm\frac{2\pi}{\sqrt{3}}, 0)$ and $k_{\mathbf{M}_2} = (\pm\frac{\pi}{\sqrt{3}}, \pm\pi)$ the interference terms become

$$\Delta\phi_{\mathbf{M}_1} = 1 - \cos[(m+n)\pi] = 1 - (-1)^{m+n},$$

$$\Delta\phi_{\mathbf{M}_2} = \begin{cases} 1 - \cos m\pi & \text{same sign} \\ 1 - \cos n\pi & \text{opposite sign} \end{cases} = \begin{cases} 1 - (-1)^m, \\ 1 - (-1)^n, \end{cases}$$

which shows that when $m + n$ is even, the van Hove singularity at $\mathbf{M}_1$ disappears by interference. In order to annihilate the $\mathbf{M}_2$ singularity, both m and n must be even. Table II summarizes the above interference physics of van Hove singularities. Figure 3 compares the impedance between points separated by a_1 that contains full DOS singularities, with a few other Z for various $ma_1 + na_2$ values, in agreement with Table II.

Outlook. We have presented a honeycomb lattice model for the circuit realization of a tilted "Dirac cone" and its local and nonlocal impedance spectroscopies to fully determine the model parameters. This promotes the impedance spectroscopy to the status of a tool to probe the emergent geometry in circuit spacetimes. Allowing the model parameters to vary on the lattice will imprint a spacetime geometry that can be arbitrarily tuned. Our model is a step towards an "on chip" realization of interesting *spacetime* geometries. The "particles" in this system are current-voltage pulses that can be traced by appropriate impedance spectroscopy whose line shape contains complete *local* information about the parameter of the model, and hence the properties of the spacetime that emerges at long distances. Our current study shows that the relation between the space group and the ensuing spacetime geometry at long distances is the same for $2p$ electrons of $8Pmmn$ borophene and current pulses. Therefore, the emergent spacetime structure of certain lattices relies on the underlying space group (lattice) more than the atoms occupying these sites. This can
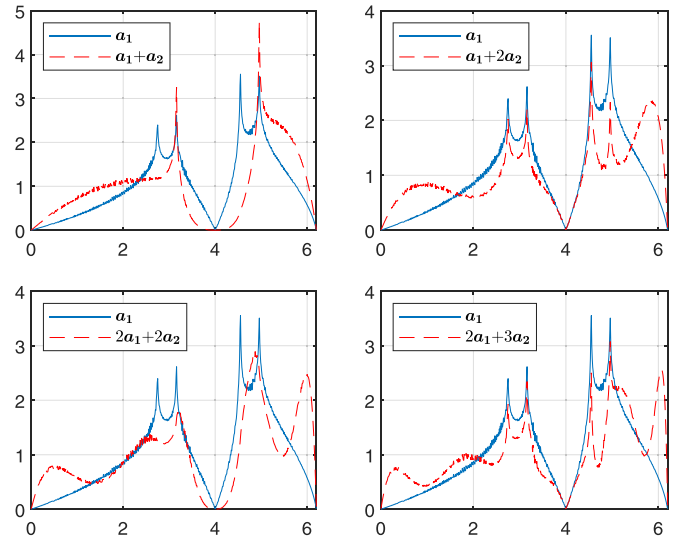

FIG. 3. The comparison between the impedance $\mathrm{Re}\{Z_{AA}(r)\}$ at $\bar{\omega}_0^2 = 4$, $c = 0.1$, $\alpha_y = -0.2$ for $r = a_1$ (blue solid curve) and $r = ma_1 + na_2$ (red dashed curve).

be a guiding principle to discover more materials with tilted Dirac cones.

The connection between graphs and *space* geometry in the context of circuit electrodynamics [24] as well as in the band theory [37] and possible implications for high-temperature superconductivity has been discussed [38]. Our proposal differs in that it offers a wider perspective for the fabrication and manipulation of *spacetime* geometry [39], not merely the space geometry [24–26]. As such, our setup allows for emulation of various "gravitational" phenomena. When one is dealing with a pure space geometry, the effect of curvature can be replaced by a pseudo $U(1)$ gauge field, while in the case of spacetime geomery, one requires non-Abelian gauge fields. As such, our circuit model can be regarded as a convenient platform for the synthesis of non-Abelian gauge fields [39].

Another important advantage of our circuit model with respect to hyperbolic lattices [24–26] is that the physically two-dimensional lattice that hosts the artificial spacetime is promoted to a graph that enjoys translational invariance. Hence, unlike the hyperbolic lattices where the concentration of circuit elements uncontrollably increases, in our model the circuit elements everywhere on the physical lattice have the same concentration. As such, three-dimensional printing technologies can be conveniently used to produce large circuits that can easily realize the continuum limit of our model.

[1] S. M. Girvin and K. Yang, *Modern Condensed Matter Physics* (Cambridge University Press, Cambridge, UK, 2019).

[2] C. H. Lee, S. Imhof, C. Berger, F. Bayer, J. Brehm, L. W. Molenkamp, T. Kiessling, and R. Thomale, Commun. Phys. **1**, 39 (2018).

[3] Y. Li, Y. Sun, W. Zhu, Z. Guo, J. Jiang, T. Kariyado, H. Chen, and X. Hu, Nat. Commun. **9**, 4598 (2018).

[4] L. H. Ryder, *Quantum Field Theory* (Cambridge University Press, Cambridge, UK, 1996).

[5] M. S. Dresselhaus, *Group Theory: Applications to the Physics of Condensed Matter* (Springer, Berlin, 2008).

[6] M. D. Schwartz, *Quantum Field Theory and the Standard Model* (Cambridge University Press, Cambridge, UK, 2014).

[7] C. Kittel, *Quantum Theory of Solids* (Wiley, New York, 1987).

[8] B. Bradlyn, J. Cano, Z. Wang, M. G. Vergniory, C. Felser, R. J. Cava, and B. A. Bernevig, Science **353**, aaf5037 (2016).

[9] Z. Zhu, G. W. Winkler, Q. Wu, J. Li, and A. A. Soluyanov, Phys. Rev. X **6**, 031003 (2016).

[10] M. I. Katsnelson, *Graphene* (Cambridge University Press, Cambridge, UK, 2012).

[11] X.-F. Zhou, X. Dong, A. R. Oganov, Q. Zhu, Y. Tian, and H.-T. Wang, Phys. Rev. Lett. **112**, 085502 (2014).

[12] A. Lopez-Bezanilla and P. B. Littlewood, Phys. Rev. B **93**, 241405(R) (2016).

[13] M. O. Goerbig, J.-N. Fuchs, G. Montambaux, and F. Piéchon, Phys. Rev. B **78**, 045415 (2008).

[14] S. Rostamzadeh, I. Adagideli, and M. O. Goerbig, Phys. Rev. B **100**, 075438 (2019).

[15] S. A. Jafari, Phys. Rev. B **100**, 045144 (2019).

[16] Z. Jalali-Mola and S. A. Jafari, Phys. Rev. B **100**, 075113 (2019).

[17] T. Farajollahpour, Z. Faraei, and S. A. Jafari, Phys. Rev. B **99**, 235150 (2019).

[18] G. E. Volovik, JETP Lett. **104**, 645 (2016).

[19] G. E. Volovik, Phys. Usp. **61**, 89 (2018).

[20] J. Nissinen and G. E. Volovik, JETP Lett. **105**, 447 (2017).

[21] L. Ryder, *Introduction to General Relativity* (Cambridge University Press, Cambridge, UK, 2009).

[22] B. Schutz, *A First Course in General Relativity* (Cambridge University Press, Cambridge, UK, 2009).

[23] A. Mohajerani, Z. Faraei, and S. A. Jafari, J. Phys.: Condens. Matter **33**, 215603 (2021).

[24] I. Boettcher, P. Bienias, R. Belyansky, A. J. Kollár, and A. V. Gorshkov, Phys. Rev. A **102**, 032208 (2020).

[25] S. K. Baek, P. Minnhagen, and B. J. Kim, Phys. Rev. E **79**, 011124 (2009).

[26] A. J. Kollár, M. Fitzpatrick, and A. A. Houck, Nature (London) **571**, 45 (2019).

[27] Y. Yekta, H. Hadipour, and S. A. Jafari, arXiv:2108.08183.

[28] M. Kardar, *Statistical Physics of Fields* (Cambridge University Press, Cambridge, UK, 2007).

[29] L. P. Kadanoff, *Statistical Physics* (World Scientific, Singapore, 2000).

[30] M. Vozmediano, M. Katsnelson, and F. Guinea, Phys. Rep. **496**, 109 (2010).

[31] See Supplemental Material at http://link.aps.org/supplemental/10.1103/PhysRevB.104.L241108 for details of some algebraic steps are provided.

[32] J. Attig and S. Trebst, Phys. Rev. B **96**, 085145 (2017).

[33] J. Attig, K. Roychowdhury, M. J. Lawler, and S. Trebst, Phys. Rev. Research **1**, 032047(R) (2019).

[34] E. N. Economou, *Greens Functions in Quantum Physics* (Springer, Berlin, 2006).

[35] J. Cserti, G. Széchenyi, and G. Dávid, J. Phys. A: Math. Theor. **44**, 215201 (2011).

[36] H. Ibach and H. Lüth, *Festkörperphysik* (Springer, Berlin, 2009).

[37] J. Maciejko and S. Rayan, Sci. Adv. **7**, 9170 (2021).

[38] G. Campi and A. Bianconi, J. Supercond. Novel Magn. **29**, 627 (2015).

[39] T. Farajollahpour and S. A. Jafari, Phys. Rev. Research **2**, 023410 (2020).